Rediscovery of Permanent Magnet Flux-Switching Machines Applied in EV/HEVs: Summary of New Topologies and Control Strategies

Gan Zhang, Wei Hua, and Ming Cheng*

(School of Electrical Engineering, Southeast University, Nanjing, 210096, China)

Abstract: Substantial efforts are currently underway around the world to develop environmentally friendly transportation, of which the development of electric vehicles plays a key role. Stator-permanent magnet (PM) machines have attracted wide attention due to the robust rotor structure and comparable performance in terms of normal permanent magnet synchronous machines (PMSM) having magnets in the rotor. In particular, the flux-switching machines feature a particular magnetic circuit configuration that favors Dy-free magnets in terms of demagnetization risk, and as a result, the cost of the motor can be reduced considerably. With focus on applications in electric vehicles (EVs) and hybrid electric vehicles (HEVs), this paper reviews the latest developments of PM flux switching machines, with particular emphasis on the novel machine topologies and control strategies.

Keywords: Electric vehicle(EV), finite element analysis, flux-switching, stator-permanent magnet.

1 Introduction

During recent years, the commercialization of NdFeB- based rare-earth permanent magnets that began in the 1980s have had significant impact on the successful development of high-performance PM machines, which are key components in so many important applications ranging from home appliances, industrial drives, electric vehicles, elevators, wind turbines, etc. The concept of mounting PMs and armature windings on stators instead of rotors, and employing double-salient structure to produce electric motors and generators predates the early 21th century, generating a new family of PM machines, i.e., the stator-PM machines[1]. Further, the stator-PM machines can be evolved into stator- excitation machines, e.g., stator-PMs or/and stator- field-excited windings. In addition, the armature windings are also on the stator, and no magnets nor windings on the rotor. As one of the three types of stator-PM machines, the flux-switching machines exhibit the advantages of high torque (power) density, large torque output capability, higher efficiency, strong irreversible demagnetization withstand capability, better thermal dissipation and liquid cooling conditions, as well as favorable high-speed operation[2-6]. It should be noted that these advantages are particularly important for electric propulsion systems, such as electric vehicles (EVs) and hybrid electric vehicles (HEVs), electric ships and more-electric aircrafts[7]. For over a decade, great efforts have been made in research of flux-witching machines, including alternative topologies[8-10], analysis methodologies[11-12], optimization designs[12-13], excitation schemes[14-15], control strategies[16-17], etc.

It is worth mentioning that the dramatic rise and fall of the price of rare-earth metals, e.g., neodymium (Nd) and dysprosium (Dy), during the period between 2010 and 2014 has led to an energetic search for alternative machine topologies to replace the high-performance PM synchronous machines (PMSMs) using sintered NdFeB magnets. Moreover, the magnets used in many currently commercialized HEVs have a certain amount of Dys in order to enhance resistance to demagnetization. In addition, [18] pointed out that the automotive applications require a cost-effective material for mass production, and Dy is known to be the most expensive heavy rare-earth in conventional Nd-based magnets. Hence, NdFeB-free or reducing the use of Dy is expected to be very cost-effective[18]. Fortunately, the flux-switching machines feature a particular magnetic circuit configuration that favors Dy-free magnets in terms of demagnetization risk.

From the perspective of EV/HEVs, this paper will review and summarize recent research work on permanent magnet flux switching (PMFS) machines, with focus on new topologies and control strategies.

2 Overlapping armature windings

Fractional-slot non-overlapping winding (NOW) is always preferred for armature windings of flux-switching machines, to achieve compact and modular structure, smaller cross-coupling between phases and shorter end-windings[19-20], which are also the main advantages of the flux-switching machines. However, challenges are associated with the application of NOW apart from harmonics and parasitic effect[20]. Firstly, it has been found that in an interior PM (IPM) machine the reluctance torque is greatly reduced due to the negligible saliency ratio by applying NOW[21-22]. Secondly, for PMFS machines with a high difference between the stator- and rotor-pole numbers, their pitch factors and hence torque density are significantly restricted by NOW connections[23]. To solve the above problems, new winding configuration possibilities for

* Corresponding Author, E-mail: huawei1978@seu.edu.cn.

Supported in part by 973 Program of China (2013CB035603), NSFC (51137001, 51322705).

PMFS machines have been proposed, e.g., the 12/7- and 6/14-pole PMFS machines with overlapping winding (OW) counterpart, where higher torque density than their NOW configuration can be achieved due to improved pitch factor[24-25]. Furthermore, a novel three-phase OW-PMFS machine with 24/16-pole combination was proposed in [26] as shown in Fig.1, as well as its NOW-counterpart, in which the air-gap permeance, flux density, saturation effect and winding inductance are analyzed using a phasor operation method and verified by finite-element analysis (FEA). It can be found that the OW and NOW configurations are based on the same stator and rotor core topology, but with considerable differences: 1) The proposed overlapping winding is a single-layer winding, while the conventional NOW is a double-layer winding. 2) The coil pitch of the OW-PMFS machine is equal to the pole pitch, bringing a pitch factor of 1. For the "one tooth-one coil" NOW-configuration, the coil pitch is smaller than the pole pitch, causing a low pitch factor of 0.5. 3) Each phase winding of the OW-PMFS machine consists of four overlapping coils, while with the NOW-PMFS machine, each phase winding is composed of eight concentrated coils.

2.1 Comparison of Static Characteristics

A pair of three-phase 24/16-pole PMFS machines with NOW- and OW-configurations respectively are compared with the well-known 12/10-pole NOW-PMFS machine[27]. The main design parameters of the three machines are given in Table 1. Clearly, to make a fair comparison, both the stack length and stator outer diameter are kept the same with that of the

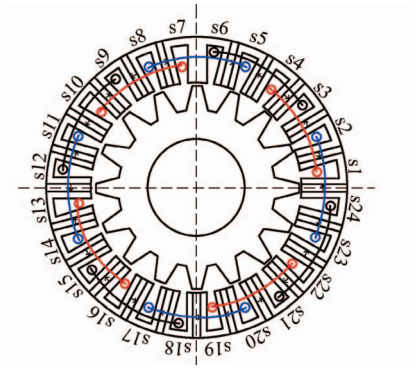

(a) Proposed overlapping windings (OW)

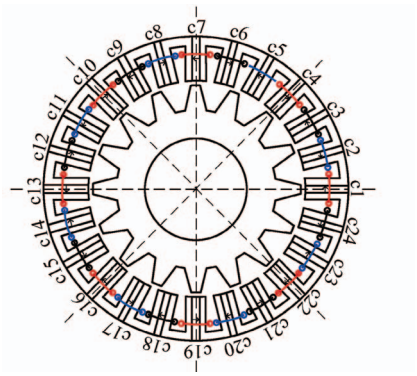

(b) Conventional non-overlapping windings (NOW)

Fig.1 Three-phase 24-stator-slot/16-rotor-pole PMFS machines with overlapping and non-overlapping windings

Table 1 Parameters of three PMFS machines with OW and NOW

Item	24/16		12/10
Winding configuration	OW	NOW	NOW
Phase number m	3		
Armature winding pole-pair p_{aw}	4		
Slots per pole per phase q	1		0.5
Rated electrical frequency f/Hz	200		
Rated rotor speed n_N/(r/min)	750		1200
Magnet remanence B_r/T	1.2		
Magnet coercivity H_c/(kA/m)	−909.46		
Rated RMS slot current density J_s/(A/mm^2)	5		
Stack length L_s/mm	75		
Stator outer radius R_{so}/mm	64		
Phase winding turns N_{ph}	280		
Coil number per phase a	4	8	4
Coil turns N_c	70	35	70
Stator split ratio k_{sio}	0.65	0.6	0.55
Air-gap length g/mm	0.35		
Stator tooth arc θ_{st}/(°)	3.75		7.5
Stator slot arc θ_{ss}/(°)	3.75		7.5
PM arc θ_{PM}/(°)	3.75		7.5
Rotor pole arc θ_{rt}/(°)	4.875	5.25	7.5
Slot area A_{slot}/mm^2	104.36	63.96×2	132.9×2

12/10-pole machine, which means the overall volume of the three machines are identical. The following comparisons are carried out based on 2D-FEA.

Fig.2 shows the open-circuit air-gap PM flux density waveforms within a coil pitch angle of the three machines. It should be noted that the curves are calculated when the PM flux linked in coil A1 reaches its peak value, i.e., the d-axis rotor position. Therefore, the magnitude of the PM coil-flux Φ_m is approximately proportional to the integral of the PM flux density along the coil pitch arc as given in Fig.2. As can be seen, the surrounding areas of the flux density curves for both of the 24/16-pole OW- and 12/10-pole NOW-PMFS machines are nearly twice that for the 24/16-pole NOW machines. Since the same turns of armature windings are adopted in each machine, the relations among their phase flux-linkage are similar to that of their coil flux[26]. Fig.3 shows that the open-circuit phase flux-linkage of the 24/16-pole NOW-FSPM machine can be effectively enhanced from 0.072Wb to 0.155Wb by adopting OW, matching the 12/10-pole NOW-PMFS design. Similar results can be found in the back-EMF of the three machines, under the electric frequency of 200Hz (Table 1), as given by Fig.4. However, the 24/16 combination suffers from large even-order harmonics in phase back-EMF (Fig.4) and high cogging torque (Fig.5) which may cause significant torque ripple as shown in the following part.

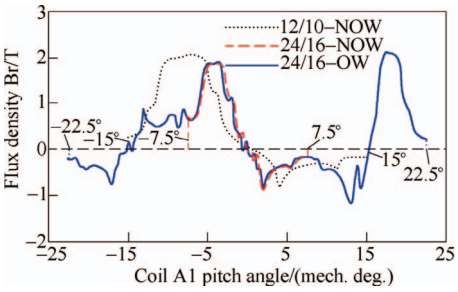

Fig.2 Open-circuit air-gap radial flux density B_r within the coil A1 pitch angle due to magnets

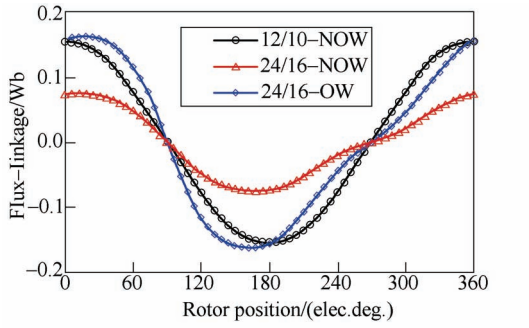

(a) Waveforms

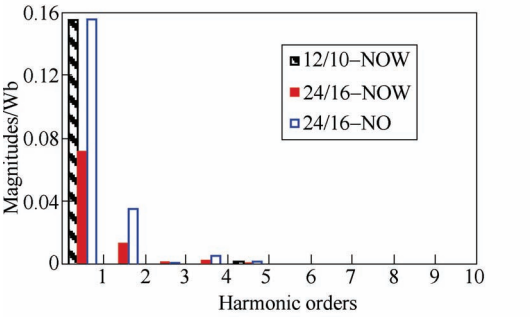

(b) Spectra

Fig.3 No-load phase flux-linkage waveforms and spectra

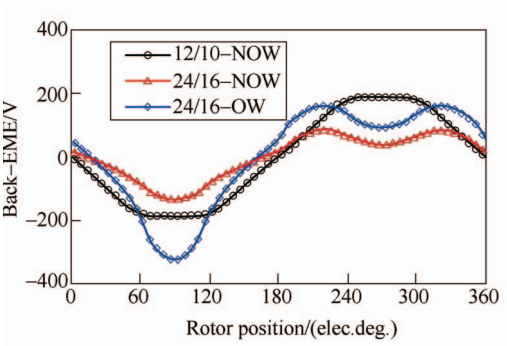

(a) Waveforms

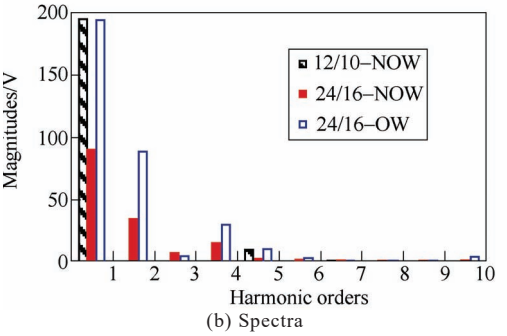

(b) Spectra

Fig.4 Open-circuit phase back-EMF (12/10-pole at 1200r/min, 24/16-pole at 750r/min)

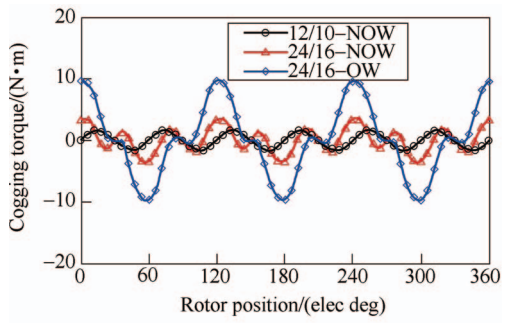

Fig.5 Cogging torque of three PMFS machines

The 2D-FEA calculated electromagnetic torque waveforms of the three machines under i_d=0 control are shown in Fig.6. It shows that the 24/16-pole OW-FSPM machine can deliver 65.2% and 17.6% respectively higher torque than that of its NOW-counterpart and the 12/10-pole NOW-FSPM machine[26]. However, the torque ripple of the 24/16-pole FSPM machine is very high, which causes severe vibration and acoustic noise and even inhibits the start of the machine. Therefore, from the perspective of machine control and design, alternative approaches have been proposed and implemented to reduce the torque ripple of the 24/16-pole OW-PMFS machine, including harmonics-current-injection (HCI) method and rotor skewing. For the HCI method[28], the injected harmonics current are deduced from the main harmonic components of torque ripple, and interacted with the *d*-axis PM flux-linkage to produce corresponding negative torque ripple components. By injecting the 3rd-, 6th-, 9th-, and 15th-order *q*-axis harmonic currents into the fundamental armature current, the torque ripple can be significantly suppressed to 54.93% as shown in Fig.7, albeit with the average torque reduced from 33.5N·m to 27.9N·m. When rotor skewing is applied, the rotor is skewed by six discrete steps to simplify the manufacture process[29]. Based on FEA, Fig.8 shows the variation of the average torque and torque ripple with the skewing angle between the adjacent two rotor segments in the 24/16-pole OW-PMFS machine. As expected, both the torque ripple and average torque are reduced with the rotor skewing. The utmost torque ripple reduction is to 4.97%. Specifically, to maintain the average torque at the level of the 12/10 design, i.e. 28.7N·m, the torque ripple can be reduced to 47.4% by rotor skewing.

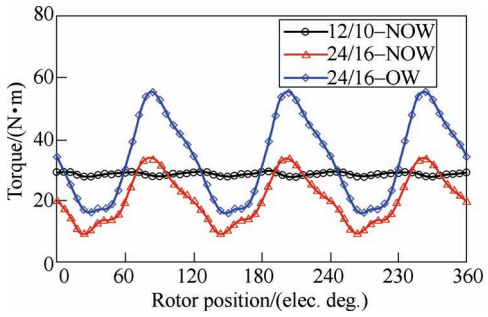

Fig.6 Comparison of torque waveforms (BLAC, i_d=0, J_s=5A/mm^2)

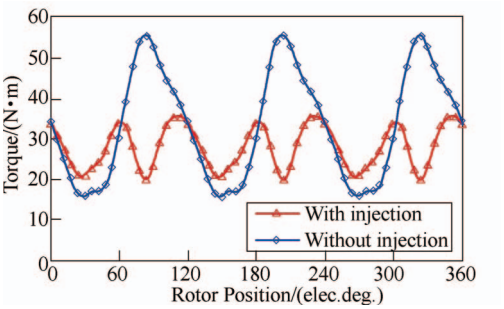

Fig.7 Torque waveforms of 24/16-pole OW-PMFS machine with and without harmonics current injection (BLAC, i_d=0, J_s=5A/mm^2)

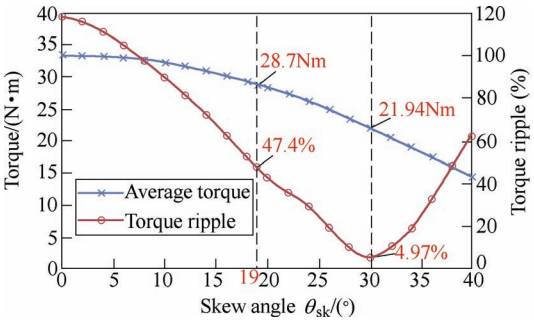

Fig.8 Effect of six-stepped rotor skewing angle on torque and torque ripple of 24/16-pole OW-PMFS machine

2.2 Experimental validations

The prototype of the proposed 24/16-pole OW-PMFS machine is fabricated and tested, as shown in Fig.9[26]. The open-circuit back-EMF waveforms are measured at 750r/min as given in Fig.10, and are compared with the 2D FEA-predicted result as shown in Fig.11. Overall, good agreements are achieved, although the measured back-EMF is nearly 15% lower than the FEA results due to end-effect, manufacturing and measuring tolerances.

3 V-shaped magnets

Recently, a new topology of PMFS machines with V-shaped magnets, called as V-shaped PMFS machines has been studied[30-31]. Fig.12(a) shows a conventional three-phase 12-stator-slot/10-rotor-pole PMFS machine and a 6/10 V-shaped PMFS machine

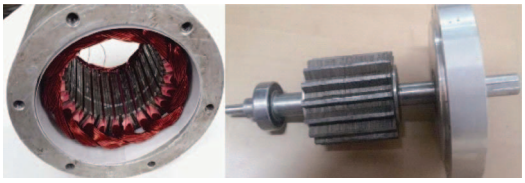

Fig.9 The 24/16-pole OW-PMFS prototype machine

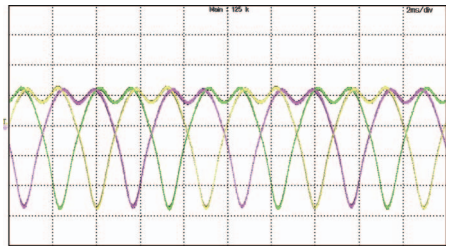

Fig.10 Measured back-EMFs of the 24/16-pole OW-PMFS prototype machine @750r/min (100V/div)

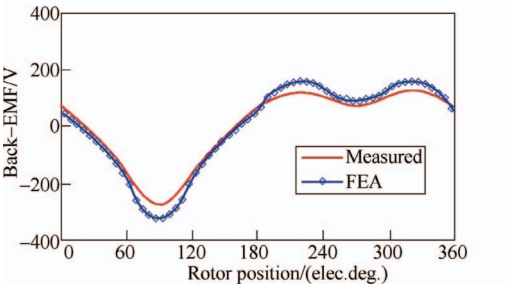

Fig.11 FE-predicted and measured phase back-EMF waveforms @750r/min of the 24/16-pole OW-PMFS prototype

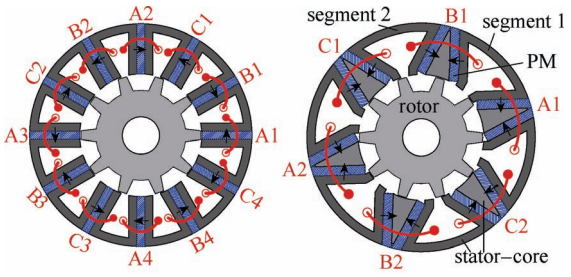

(a) 12/10, conventional (b) 6/10, V-shaped

Fig.12 The conventional and V-shaped PMFS machines

[4], which is deduced directly from the 12/10 PMFS machine by forcing two adjacent coils to be connected together. However, the torque ripple of the resultant 6/10 V-shaped machine reaches 58% (the average torque is 3.96N·m and the torque fluctuations are between 2.8Nm and 5.1N·m), and the back-EMF is asymmetrical, since the two adjacent coils in the conventional 12/10 PMFS machine belong to different phase windings, such as A1 and B1. Hence, the 6/10 combination is not optimal for V-shaped PMFS machines. In [32], a novel 6/17 V-shaped PMFS machine is proposed based on conventional 12/17 topology, which exhibits more sinusoidal back-EMF waveform and smaller torque ripple. Furthermore, two variants of 6/17 V-shaped machines are developed to improve the performances further, e.g., larger torque, less torque ripple, and easier mechanical processing.

3.1 V-shaped PMFS machine topology

For the V-shaped PMFS machines, each stator pole is composed of two pieces of magnets with opposite magnetizations, and can be regarded as a connection of two adjacent stator poles of typical PMFS machines. Hence, the two adjacent coils of the typical PMFS machines should belong to the same phase winding, namely, the coils connection of "AABBCC", e.g., as in the 12/11 (shown in Fig.13) and 12/13 combinations. Another combination is 12/17, whose coil-EMF vectors and coils connection are shown in Fig.14. Although the 12/11 and 12/17 adopts the same winding compositions, the coils in these two machine have different polarities. For the 12/11 one, the two adjacent coils are of opposite polarities, e.g., coils A1 and A2 as shown in Fig.13(c). While for the 12/17 one, the two adjacent stator coils are of the same polarity. As a result, the sum of the magneto-motive-force (MMF) due to armature currents in the stator slot between stator poles 1 and 2 is always zero since the currents injected into the

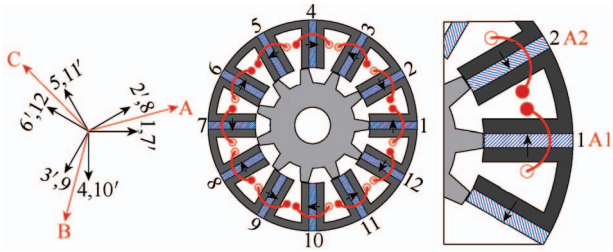

(a) Coil-EMF vectors (b) Coils connection (c) Details

Fig.13 Coil-EMF vectors and coils connection of a typical 12/11 PMFS machine

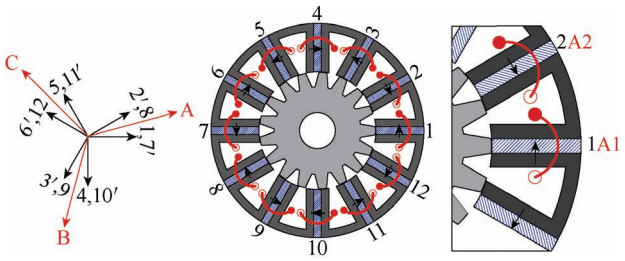

(a) Coil-EMF vectors (b) Coils connection (c) Details

Fig.14 Coil-EMF vectors and coils connection of a typical 12/17 PMFS machine

corresponding stator slots can be cancelled. Therefore, the relative stator slots are eliminated to form a 6/17 V-shaped PMFS machine as shown in Fig.15(a), where the stator consist of six stator coils, six pairs of PMs, six horseshoes-shaped laminated segments, and six triangular laminated segments[32].

Fig.15(b) shows the FEA-predicted three-phase back-EMF waveforms. Obviously, the phase back-EMF is symmetrical and quasi-sinusoidal with a total harmonic distribution (THD) of 6.96%. In the following analysis, the *d*-axis current is i_d=0, namely the reluctance torque is neglected. Fig.15(c) shows the electromagnetic torque versus rotor position of the 6/17 V-shaped machine with a current density of J_{sa}=5A/mm^2 and a slot package factor of k_{pf}=0.45. The average torque is 10.15N·m and the torque ripple is 11.4%, much less than the 6/10 V-shaped counterpart.

3.2 Performance improvement for the 6/17 machine

Although the torque ripple of the above 6/17 V-shaped machine is considerably suppressed compared with the 6/10 machine, several problems still exist. Firstly, the stator core is divided into 6 horseshoes-shaped segments and 6 triangular segments, which results in difficulty in mechanical processing. Secondly, although the torque ripple has been reduced to 11.4%, it is still unsuitable for smooth torque. Hence, two improved variants based on the above mentioned 6/17 V-shaped machine are developed [32].

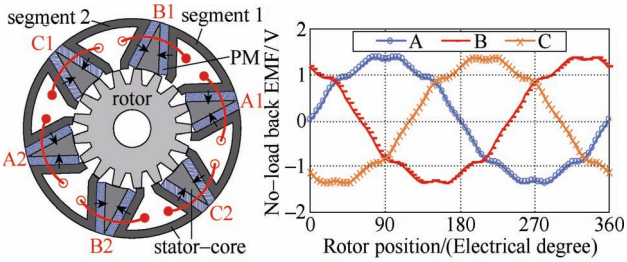

(a) Cross-section (b) Back-EMF waveforms at 1500r/min

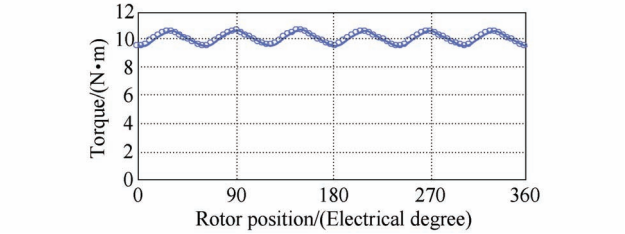

(c) Electromagnetic torque (J_{sa}=5A/mm^2 and k_{pf}=0.45).

Fig.15 Topology and performance of an original 6/17 V-shaped PMFS machine

Observing the 6/17 V-shaped machine, the polarities of horseshoes-shaped segments on both sides of the V-shaped PMs are the same and the PM fluxes always flow from the horseshoes-shaped segments to the triangular segments, such as segments 1 and 2, illustrated in Fig.15(a). Therefore, the six horseshoes- shaped segments can be connected into a united stator iron as shown in Fig.16(a) and termed as "variant 1". It can be seen that the stator core of variant 1 is comprised of a united stator yoke (stator-core 1) and six triangular laminated segments (stator-core 2). Considering that the stator-core 2 is difficult to be fixed on the stator, the magnetic bridges with a width of 1mm are introduced, forming another improved variant with entity stator core as shown in Fig.16(b) and termed as "variant 2".

In [32], comprehensive comparisons of electromagnetic performances, including unbalanced magnetic force, back-EMF per turn, electromagnetic torque, torque ripple, and efficiency, are also conducted among the three V-shaped machines. Specifically, as can be seen in Fig.17, the amplitude of phase back-EMF per turn of variant 1 is remarkably larger than the other two machines since the phase PM flux of variant 1 is strengthened by flowing through stator yoke, whereas variant 2 suffers from considerably unfavorable flux leakage due to the magnetic bridges. The THD values of phase back-EMF waveforms are 6.96%, 5.69% and 2.21%, respectively for the original one, variant 1, and variant 2, indicating the back-EMF harmonics of variant 2 are smallest.

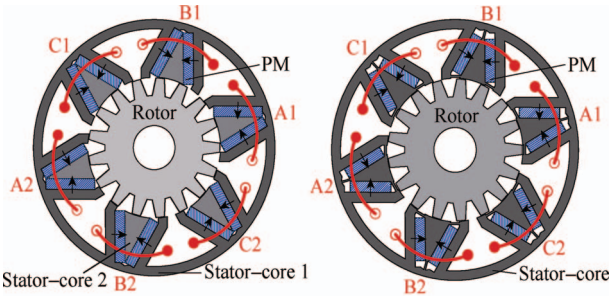

(a) Variant 1 (b) Variant 2

Fig.16 Two variants of the 6/17 V-shaped PMFS machine

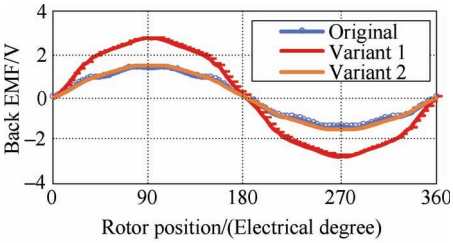

(a) Phase back-EMF waveforms at 1500r/min

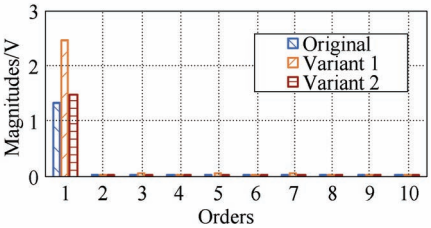

(b) Harmonics.

Fig.17 Topology and performance of an original 6/17 V-shaped PMFS machine

Fig.18 shows the electromagnetic torque waveforms of three V-shaped machines when armature current density is J_{sa}=5A/mm^2 (k_{pf}=0.45) under i_d=0 control. It can be found that the average torque and torque ripple of the original 6/17 machine is 10.15N·m and 11.4%, respectively. However, for variant 1, the average torque can be improved to 15.03Nm, being higher than the original machine by 48% even under i_d=0 control, whereas the torque ripple is a little larger, being 13.1%. For variant 2, the average torque is 10.23N·m, which is slightly larger than the original machine (10.15N·m), and the torque ripple is only 4.3%, which is the least among the three V-shaped machines. Fig.18(b) shows that the torques of the original machine and variant 2 are quite close, and are always lower than that of variant 1.

4 Outer-Rotor PMFS Machine with Wedge-Shaped Magnets

4.1 Outer-rotor PMFS machines having stator-PM

With regard to electric vehicles, there is a trend of using in-wheel motors due to their high torque density, structural compactness, and maintenance-free requirements. Certainly, the PMFS machine is a good candidate for in-wheel applications, especially considering its simple and robust rotor structure.

In fact, the outer-rotor stator-permanent-magnet flux-switching (OR-SPM-FS) machines are directly inherited from the outer-stator PMFS (OS-PMFS) machines and proposed for light traction applications in [33] and [34], where the inner-stator magnets are rectangular-shaped as that of traditional outer-stator topologies. However, it is found that rectangular is not the optimal magnet shape especially for the in-wheel OR-SPM-FS machines since the inner-stator armature winding slots will be squeezed by the bottom of magnets and stator teeth where the magnetic saturation is light. Hence, an OR-SPM-FS machine with wedge-shaped magnets is proposed in [35], as shown in Fig.19 and Fig.20.

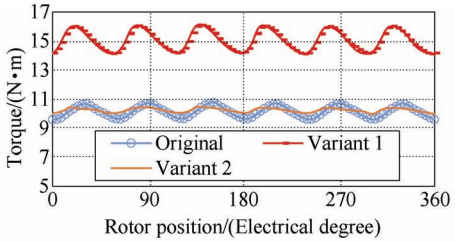

(a) Electromagnetic torque waveforms under J_{sa}=5A/mm^2

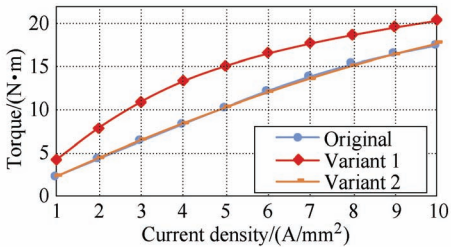

(b) Electromagnetic torque waveforms versus current densities

Fig.18 Performance comparisons among three machines

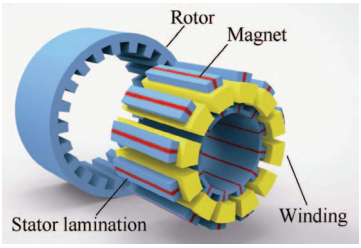

Fig.19 A three-phase 12-stator-slot/22-rotor-pole outer-rotor stator-PM flux-switching (OR-SPM-FS) machine

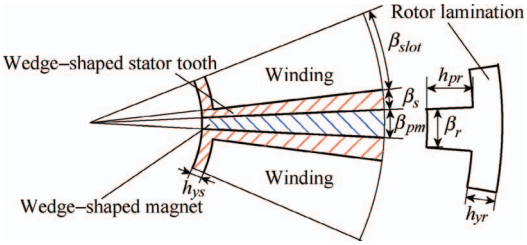

Fig.20 Key dimensions of an OR-SPM-FS machine with wedge-shaped magnets

In [35], the combinations of stator slot and rotor pole numbers are investigated and optimized to achieve high electromagnetic torque and low torque ripple. Moreover, the analytical torque-sizing and winding resistance prediction equations are derived to demonstrate the relationship between performance and dimensions. Based on the foregoing literature and 2D-FEA methods, the key geometric parameters are optimized to achieve high average torque and low torque ripple. Furthermore, comprehensive comparisons of electromagnetic performance, including efficiency, flux-weakening and loading capabilities, etc., are conducted between a pair of OR-SPM-FS machines with rectangular- and wedge-shaped magnets. The results indicate that the OR-SPM-FS with wedge-shaped magnets exhibits superior torque performance, better flux-weakening capability, higher efficiency, and wider speed range. Finally, the predicted performance of the proposed OR-SPM-FS machine are validated by experiments on a prototyped machine, as shown in Fig.21 and Fig.22.

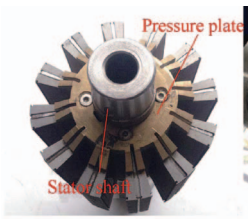

(a) Stator without coils

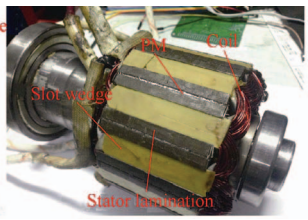

(b) Stator

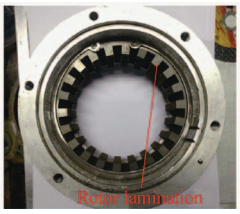

(c) Rotor

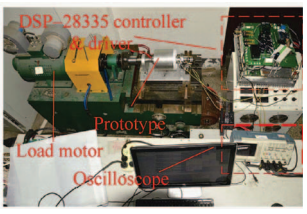

(d) Experimental platform

Fig.21 Prototyped machine and experimental platform configuration of the OR-SPM-FS machine

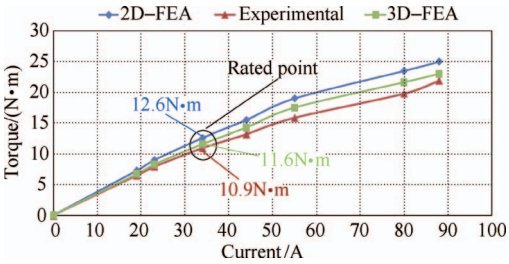

Fig.22 Average torque versus phase current (peak value) at 120r/min of the OR-SPM-FS machine

4.2 Outer-rotor PMFS machines having rotor-PM

Significant saturation in the stator teeth is normally inevitable in outer-rotor SPM-FS machines, hence, a novel outer-rotor flux-switching machine having magnets in rotor instead of stator is firstly proposed in [36], and is named as outer-rotor rotor-PM flux- switching (OR-RPM-FS) machine as shown in Fig.23. In the OR-RPM-FS machine, the stator consists of the stator laminations and armature windings, similar to a conventional rotor-PM machine. The magnets are located on the rotor and circumferentially magnetized in same directions, resulting in a sandwich structure of "tooth-PM-tooth" where the nonmagnetic support cells are set to support the rotor teeth and magnets. This machine inherits the "flux-switching" principle from conventional stator-PM PMFS machine, by moving magnets from stator to rotor.

In [36], a comprehensive comparison of back-EMF, inductance, torque capability, efficiency, and flux-weakening capability between OR-RPM-FS machine and OR-SPM-FS machine is conducted. The results indicate that OR-RPM-FS machine has better torque capability and higher efficiency, but weaker flux-weakening capability than OR-SPM-FS machine, as shown in Fig.24.

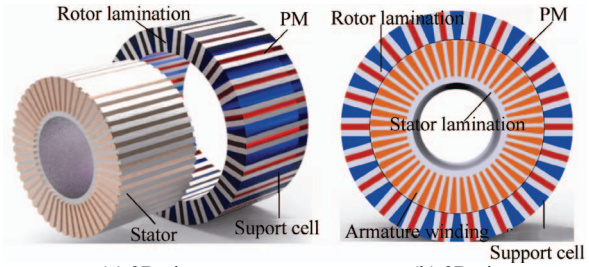

(a) 3D view (b) 2D view

Fig.23 Three-phase 48/22 outer-rotor rotor-PM flux-switching (OR-RPM-FS) machine

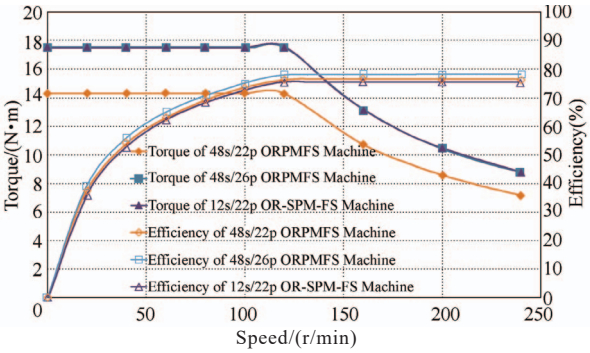

Fig.24 Average torques and efficiency versus speed of different outer-rotor permanent magnet brushless machines

5 Co-axial dual-mechanical-port PMFS machine

Substantial efforts are invested in development of pure electric, hybrid, and extender-based hybrid vehicles. Among them, the fuel-based extended-range electric vehicles (ER-EVs) show advantages of high endurance ability, high efficiency and low battery capacity required. In conventional ER-EVs, the generator and the traction motor are independent, and can be laterally placed in the front of the vehicle together, or respectively placed at both ends of the vehicle. However, both configurations will reduce space and create potential heat dissipation problems. To overcome the disadvantages, a novel co-axial dual-mechanical-port PMFS (CADMP- PMFS) machine is proposed in [37], as shown in Fig.25, where it is axially composed of an inner-rotor PMFS machine, an outer-rotor PMFS machine, and a magnetic-isolation ring between them. The CADMP- PMFS machine-based power train system is shown in Fig.26. The inner PMFS machine works as a generator to charge the batteries, which provides energy to the outer machine by the converter to drive the vehicle directly.

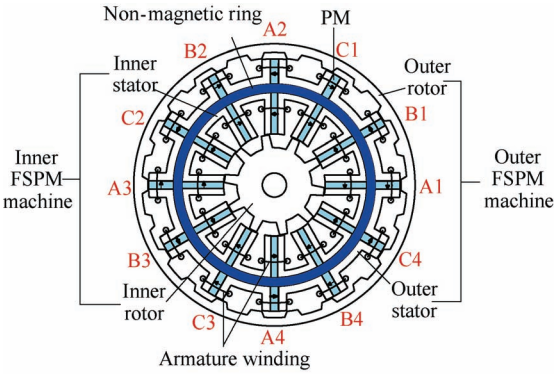

(a) Cross section

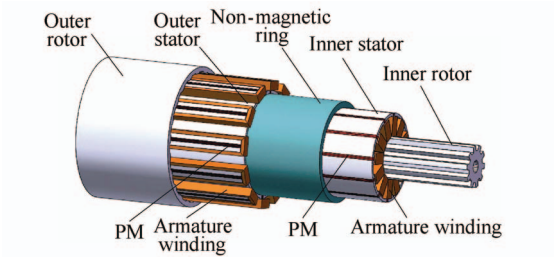

(b) 3-D model

Fig.25 Structure of the CADMP-PMFS machine

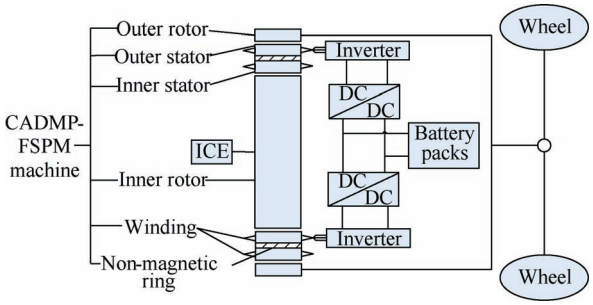

Fig.26 The configuration of the CADMP-PMFS machine based ER-EV

Additionally, the electromagnetic performance and power-dimension equations of the CADMP-PMFS machine are also given in [37], with more attention paid to the isolation ring. The main advantage of this machine is the robust rotor structure of both inner and outer PMFS machines.

6 Torque Ripple Minimizing Methods

For the PMFS machines, due to the high airgap flux density produced by magnets and the special double salient structure, the cogging torque is relatively large, resulting in unfavorable torque and speed ripples. Existing methods to minimize the torque ripple can be briefly categorized into two types: the machine-based and the control-based. The first method concentrates on the design and optimization of the machine itself, such as additional dummy slot structure[38], stator/rotor skewing[39], tooth chamfering[40], rotor step skewing[41], etc. While the second one consists of harmonic-current- injection based active control schemes[42-43].

6.1 Machine-based method

From the perspective of machine-based methods, adjusting the rotor dimensions in PMFS machine is highly recommended to minimize cogging torque since its rotor is relatively simple. Therefore, numerous scholars try to suppress the cogging torque of PMFS machines by optimizing the rotor tooth arc width during the machine design stage[40-41]. Various rotor tooth shapes to minimize the cogging torque have been introduced, including notched teeth, eccentric teeth, and stepped teeth, etc.[44]. However, it should be noted that the average electromagnetic torque in these literatures will be reduced remarkably. In fact, almost all the techniques proposed previously to achieve the goal of cogging torque reduction inevitably result in the loss of average electromagnetic torque to some extent. In [45], two different tooth chamfering types, i.e., circular bead and right angle are presented, as shown in Fig.27. Clearly, both chamfering types can be employed not only in stator side but also in rotor side. Hence, there are quite a lot of possible combinations and they are listed in Fig.28.

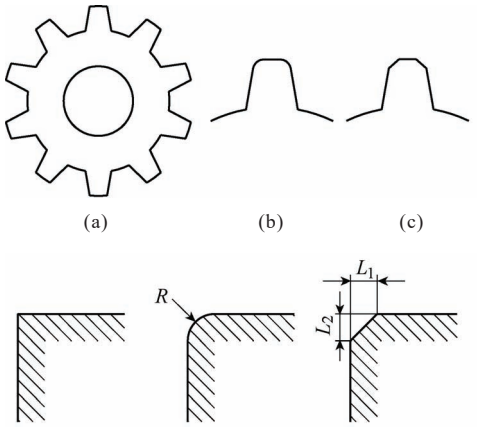

Fig.27 The rotor tooth-chamfering types

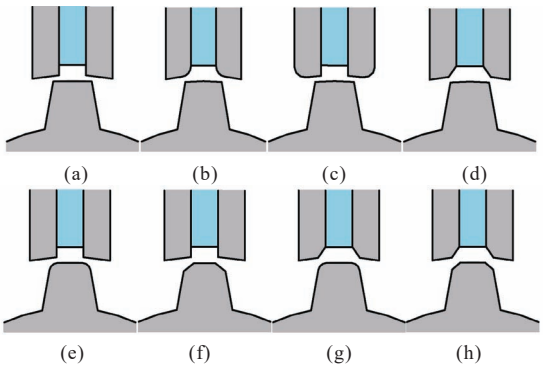

Fig.28 Various combinations of tooth chamfering both in stator and rotor teeth

Based on FEA, the cogging torque waveforms are given in Fig.29, where a~h corresponding to tooth-chamfering types shown in Fig.2. Specifically, Fig.28(a) and Fig.29(a) indicate the original machine without tooth chamfering. As can be seen, only the cases of (f), (g), and (h) result in the reduction of cogging torque. Interestingly, the circular bead in tooth appears to be more effective than right angle, when comparing Fig.29(e) and (f). This is mainly due to the different distribution of air-gap permeance. Overall, Fig.29(g) and (h) shows satisfactory cogging torque minimization results.

From the above analyzes, case (h) has the most effective cogging torque reduction. Fig.30 presents the back-EMF and average torque waveforms when

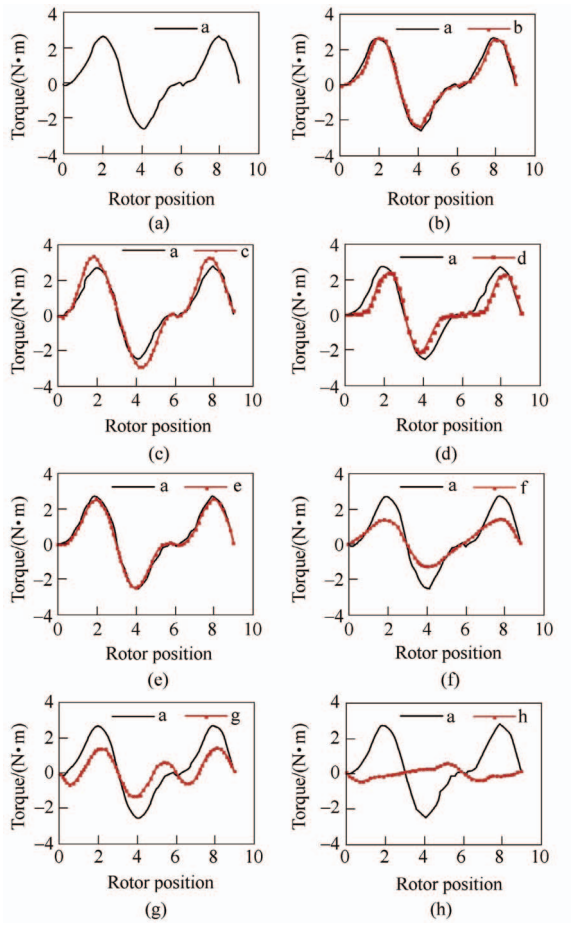

Fig.29 Cogging torque waveforms of various tooth-chamfering combinations

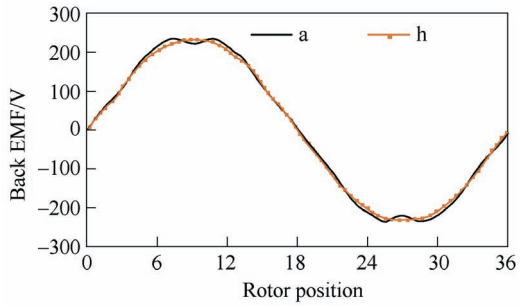

(a) Phase back-EMF at 1200r/min

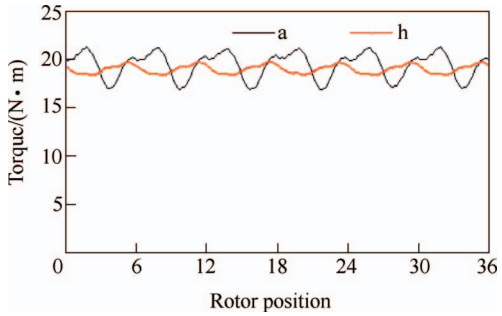

(b) Electromagnetic torque waveform at I_m=5A rms

Fig.30 Electromagnetic performance when loaded

case h is utilized. The results indicate that employing this approach helps to achieve a more sinusoidal back-EMF waveform and reduce the torque ripple, while maintaining the average torque output.

6.2 Control-based method

The machine-based method can reduce the torque ripple to some extent, but may result in increased manufacturing cost and decreased performance. The control-based method focuses on the control side such as compensation control[46] and iterative learning control (ILC)[47]. The typical approach of the compensation control is injecting compensating harmonic currents or voltages into a three-phase PMFS machine to generate additional torque components counteracting the cogging torque. The main idea of the ILC is to improve the tracking performance of systems that operate repetitively over a fixed time interval. Actually, the ILC is an error correction algorithm and memory that stores previous controller output data and error information[47].

High performance control of machine drives includes both steady-state and dynamic behaviors. Apart from the low torque ripple, the satisfactory transient performance should be taken into account as well. As a possible strategy to improve the dynamic behaviors of machine drives, model predictive control (MPC) has been widely researched, and the most popular type is the finite-control set MPC (FCS-MPC)[48-52]. According to the control variables, the MPC strategy can be categorized into three types, namely, model predictive current control (MPCC)[51], model predictive torque control (MPTC)[48], and model predictive flux control (MPFC)[52]. Very recently, some researchers have extended the MPC method into the PMFS machine control. In [51], a fully-decoupled model predictive control scheme with fixed switching frequency is developed to improve the dynamic performance of a nine-phase PMFS machine, however, the cogging torque has not been considered.

Recently, based on the MPCC method and the compensation control theory, a compensating-current MPCC (CC-MPCC) scheme is proposed and implemented to counteract the dominant components in cogging torque of an existing three-phase 12/10 PMFS prototyped machine[53] to alleviate the influence of the cogging torque and improve the smoothness of electromagnetic torque and speed, where a comprehensive cost function is designed to evaluate the switching states. The structure and flow diagram are shown in Fig.31 and Fig.32, respectively. The experimental results in Fig.33(a) indicate that the CC-MPCC scheme can suppress the torque ripple significantly by comparisons with the conventional MPCC strategy. The start-up response in Fig.33(b) demonstrates the proposed method can also offer satisfactory dynamic performances.

In [54], a developed MPFC strategy with P-type ILC is proposed and implemented for a three-phase PMFS machine, aiming at torque ripple minimization. The transformation process of the stator flux reference is simplified by using only the references of stator flux amplitude and torque angle. Moreover, P-type ILC as shown in Fig.34 is adopted to alleviate the impact of cogging torque. The structure of the developed MPFC with P-type ILC is presented in Fig.35. The proposed control strategy inherits the merits of MPFC and P-type ILC. The experimental results in Fig.36 reveal that the proposed MPFC combining ILC strategy can suppress the torque ripple and improve dynamic performance.

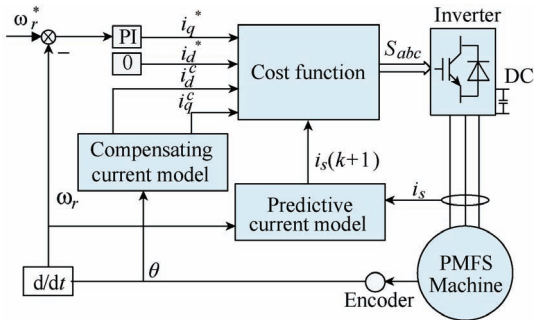

Fig.31 Control block diagram of CC-MPCC scheme

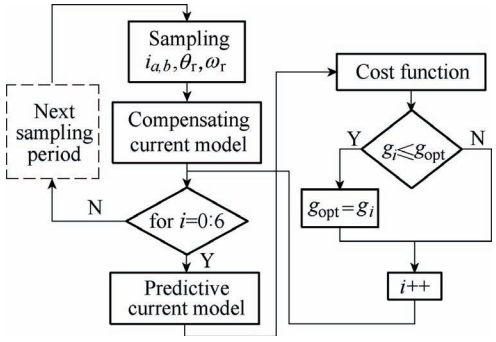

Fig.32 Flow diagram of CC-MPCC scheme

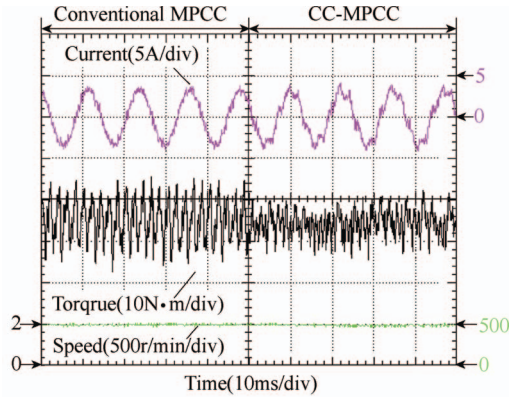

(a) Steady-state performance

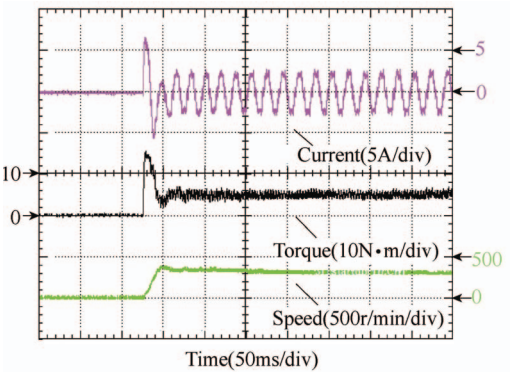

(b) Response to start-up

Fig.33 Measured phase current, torque and speed waveforms of CC-MPCC

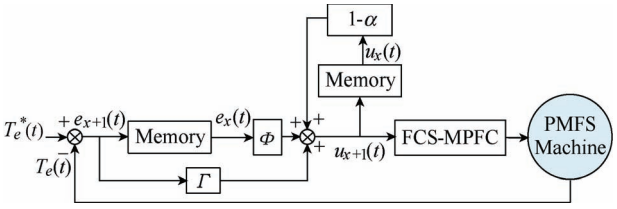

Fig.34 P-type ILC structure

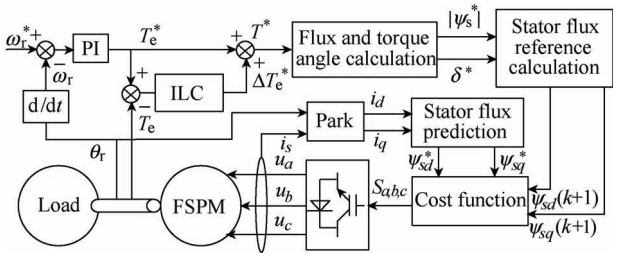

Fig.35 The structure of the developed MPFC for torque ripple minimization

The above two control methods can alleviate the influence of the cogging torque and enhance transient performance. But the main theory of the two methods are different. The compensating-current model of the CC-MPCC is based on the mathematical model of the cogging torque. As the developed MPFC with ILC scheme employs an additional controller, resulting in more parameters for tuning, this may increase the difficulty and complexity of implementation.

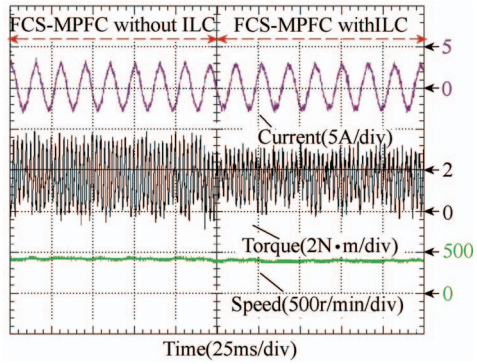

(a) Steady-state performance

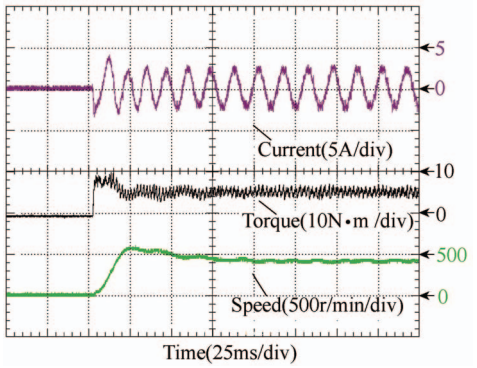

(b) Response to start-up

Fig.36 Measured phase current, torque and speed waveforms of the developed MPFC with ILC

7 Conclusion

The study on flux-switching machines has been widely carried out for over a decade and is always influenced by the price of rare-earth materials. Instead of DC-excited or hybrid excited (DC and PM) flux switching machines, the permanent magnet flux- switching (PMFS) machines still have significant potential in EV/HEV related applications, especially considering that their special magnetic circuit feature favoring Dy-free magnets in terms of demagnetization risk. Hence, from the perspective of EV/HEVs, this paper summarizes recent investigations on PMFS machines, including new topologies and control methods. The outer rotor and dual-mechanical-port PMFS machines are also introduced, which aim to integrate power dividing devices in HEVs.

References

[1] M. Cheng, W. Hua, J. Z. Zhang, and W. X. Zhao, "Overview of stator- permanent magnet brushless machines," *IEEE Trans. Ind. Electron.*, vol. 58, no. 11, pp. 5087-5101, Mar. 2011.

[2] W. Hua, M. Cheng, and G. Zhang, "A novel hybrid excitation flux-switching motor for hybrid vehicles," *IEEE Trans. Magn.*, vol. 45, no. 10, pp. 4728-4731, Oct. 2009.

[3] Z. Q. Zhu, and J. T. Chen, "Advanced flux-switching permanent magnet brushless machines," *IEEE Trans. Magn.*, vol. 50, no. 11, pp. 1447-1453, Jun. 2010.

[4] M. Y. Lin, L. Hao, and X. Li, "A novel axial field flux-switching permanent magnet wind power generator," *IEEE Trans. Magn.*, vol. 47, no.10, pp. 4457-4460, Oct. 2011.

[5] W. Hua, G. Zhang, and M. Cheng, "Flux-regulation theories and principles of hybrid-excited flux-switching machines," *IEEE Trans. Ind. Electron.*, vol. 62, no. 9, pp. 5359-5369, Sep. 2015.

[6] G. Zhang, W. Hua, M. Cheng, and J. G. Liao, "Design and comparison of two six-phase hybrid-excited flux-switching machines for EV/HEV applications," *IEEE Trans. Ind. Electron.*, vol. 63, no. 1, pp. 481-493, Jan. 2016.

[7] K. T. Chau, C. C. Chan, and C. Liu, "Overview of permanent-magnet brushless drives for electric and hybrid electric vehicles," *IEEE Trans. Ind. Electron.*, vol. 55, no. 6, pp. 2246-2257, Jun. 2008.

[8] S. E. Abdollahi, and S. V. Zadeh, "Back EMF analysis of a novel linear flux switching motor with segmented secondary," *IEEE Trans. Magn.*, vol. 50, no.4, pp. 8200890, Apr. 2014.

[9] Y. B. Wang, M. Chen, T. W. Ching, and K. T. Chau, "Design and analysis of a new HTS axial-field flux-switching machine," *IEEE Trans. Appl. Supercond.*, vol. 25, no.3, pp. 5200905, Jun. 2015.

[10] C. S. Walter, H. Polinder, and J. A. Ferreira, "High-torque-density high-efficiency flux-switching PM machine for aerospace applications," *IEEE Journal of Emerging and Selected Topics in Power Electronics*, vol. 1, no. 4, pp. 327-336, Dec. 2013.

[11] C. C. Hwang , C. M. Chang , S. S. Hung , and C. T. Liu, "Design of high performance flux switching PM machines with concentrated windings," *IEEE Trans. Magn.*, vol. 50, no. 1, pp. 4002404, Jan. 2014.

[12] Y. Du, F. Xiao, W. Hua, X. Y. Zhu, M. Cheng, L. Quan, and K. T. Chau, "Comparison of flux-switching PM motors with different winding configurations using magnetic gearing principle," *IEEE Trans. Magn.*, vol. 52, no. 5, pp. 8201908, May 2016.

[13] W. Z. Fei, P. C. K. Luk, D. M. Miao, and J. X. Shen, "Investigation of torque characteristics in a novel permanent magnet flux switching machine with an outer-rotor configuration," *IEEE Trans. Magn.*, vol. 50, no. 4, pp. 8100810, Apr. 2014.

[14] A. Dupas, S. Hlioui, E. Hoang, M. Gabsi, and M. Lecrivain, "Investigation of a new topology of hybrid-excited flux-switching machine with static global winding: experiments and modeling," *IEEE Trans. Ind. Appl.*, vol. 52, no. 2, pp. 1413-1421, Mar./Apr. 2016.

[15] S. M. Yang, J. H. Zhang, and J. Y. Jiang, "Modeling torque characteristics and maximum torque control of a three-phase, DC-excited flux-switching machine," *IEEE Trans. Magn.*, vol. 52, no. 7, pp. 8104204, Jul. 2016.

[16] R. P. Deodhar, A. Pride, S. Iwasaki, and J. J. Bremner, "Performance improvement in flux-switching PM machines using flux diverters," *IEEE Trans. Ind. Appl.*, vol. 50, no. 2, pp. 973-978, Mar./Apr. 2014.

[17] F. Lin, K.T. Chau, C. H. T. Lee, and C. H. Liu, "Fault signature of a flux-switching DC-field generator," *IEEE Trans. Magn.*, vol. 51, no. 11, pp. 8206304, Nov. 2015.

[18] T. Raminosoa, A. M. El-Refaie, D. Pan, K. K. Huh, J. P. Alexander, K. G. Grace, S. Grubic, S. Galioto, P. B. Reddy; and X. C. Shen, "Reduced rare-earth flux-switching machines for traction applications," *IEEE Trans. Ind. Appl.*, vol. 51, no. 4, pp. 2959-2971, Jul./Aug. 2015.

[19] J. Cros, and P. Viarouge, "Synthesis of high performance PM motors with non-overlapping windings," *IEEE Trans. Energy Convers.*, vol. 17, no. 2, pp. 248-253, Jun. 2002.

[20] A. El-Refaie, "Fractional-slot concentrated-windings synchronous permanent magnet machines: opportunities and challenges," *IEEE Trans. Ind. Electron.*, vol. 57, no. 1, pp. 107-121, Jan. 2010.

[21] J. K. Tangudu, T. M. Jahns, and A. El-Refaie, "Unsaturated and saturated saliency trends in fractional-slot concentrated-winding interior permanent magnet machines," *in Proc. Energy Conversion Congress and Exposition (ECCE), 2010 IEEE*, pp. 1082–1089, Sept. 2010.

[22] X. Zhang, R. Qu, H. Chen, and J. Luo, "Analysis of d- and q-axis inductances and saliency ratios in interior permanent magnet machines with fractional-slot concentrated windings considering harmonic effects," *in Proc. 2013 Int. Conf. on Electrical Machines and Systems (ICEMS)*, pp. 1080-1085, Oct. 2013.

[23] J. T. Chen, and Z. Q. Zhu, "Winding configurations and optimal stator and rotor pole combination of flux-switching PM brushless AC machines," *IEEE Trans. Energy Convers.*, vol. 25, no. 2, pp. 293-302, Jun. 2010.

[24] F. Xiao, Y. Du, W. Hua, M. Cheng, Y. Sun, H. Zhu, and T. Ching, "Winding configuration design of flux-switching PM motors based on magnetic gearing principle," *in Proc. Magnetics Conference (INTERMAg2015)*, May 2015.

[25] D. Li, R. Qu, J. Li, W. Xu, and L. L. Wu, "Synthesis of flux switching permanent magnet machines," *IEEE Trans. Energy Convers.*, vol. 31, no. 1, pp. 106-117, Mar. 2016.

[26] L. Y. Shao, W. Hua, Z. Q. Zhu, X. F. Zhu, M. Cheng, and Z. Z. Wu, "A novel flux-switching permanent magnet machine with overlapping windings," *IEEE Trans. Energy Convers.*, 2016, Early access.

[27] W. Hua, and M. Cheng, "Static characteristics of doubly-salient brushless machines having magnets in the stator considering end-effect," *Electric Power Components and Systems*, vol. 36, no. 7, pp. 754-770, Jun. 2008.

[28] H. Jia, M. Cheng, W. Hua, W. Zhao, and W. Li, "Torque ripple suppression in flux-switching PM motor by harmonic current injection based on voltage space-phasor modulation," *IEEE Trans. Magn.*, vol. 46, no. 6, pp. 1527-1530, Nov. 2010.

[29] W. Fei, P. C. K. Luk, and J. Shen, "Torque analysis of permanent-magnet flux switching machines with rotor step skewing," *IEEE Trans. on Magn.*, vol. 48, no. 10, pp. 2664-2673, Oct. 2012.

[30] Y. J. Zhou, and Z. Q. Zhu, "Torque density and magnet usage efficiency enhancement of sandwiched switched flux permanent magnet machines using V-shaped magnets," *IEEE Trans. on Magn.*, vol. 49, no. 7, pp. 3834-3837, Jul. 2013.

[31] L. H. Mo, L. Quan, Y. Y. Chen, and H. B. Qiu, "Sandwiched flux- switching permanent-magnet brushless AC machines using V-shape magnets," *IEEE Vehicle Power and Propulsion Conference (VPPC)*, pp. 1-5, 2013.

[32] G. S. Zhao, and W. Hua, "A novel flux-switching permanent magnet machine with v-shaped magnets," *AIP Advances*, 2016, Accpeted.

[33] W. Fei, P. C.K. Luk, J.X. Shen, Y. Wang, and M. Jin, "A novel permanent-magnet flux switching machine with an outer-rotor configuration for in-wheel light traction applications," *IEEE Trans. Ind. Appl.*, vol.48, no.5, pp.1496-1506, Sep./Oct. 2012.

[34] W. Fei, P. C. K. Luk, D. M. Miao, and J. X. Shen, "Investigation of torque characteristics in a novel permanent magnet flux switching machine with an outer-rotor configuration," *IEEE Trans. Magn.*, vol. 50, no. 4, pp1-10, Apr. 2014.

[35] W. Hua, H. L. Zhang, M. Cheng, J. J. Meng, and C. Hou, "An outer-rotor flux-switching permanent magnet machine with wedge-shaped magnets for in-wheel light traction," *IEEE Trans. Ind. Electron.*, vol. 64, no. 1, pp.69-80, Jan. 2017.

[36] H. L. Zhang, and W. Hua, "A novel outer-rotor-permanent-magnet flux-switching machine for in-wheel light traction," *in proceedings of 42nd Annual Conference of IEEE Industrial Electronics Society*, pp. 6633-6638, Florence, Italy, 2016.

[37] L. K. Zhou, W. Hua, and G. Zhang, "Power distribution of a co-axial dual-mechanical-port flux-switching permanent magnet machine for fuel-based extended range electric vehicles," *AIP Advances*, 2016, Accpeted.

[38] W. Hua, and M. Cheng, "Cogging torque reduction of flux-switching permanent magnet machines without skewing," in *International Conference on Electrical Machines and Systems*, Wuhan, China, pp. 3020-3025, 2008.

[39] M. J. Jin, Y. Wang, J. X. Shen, P. C. K. Luk, W. Z. Fei, and C. F. Wang, "Cogging torque suppression in a permanentmagnet flux-switching integrated-starter-generator," *IET Electric Power Applications*, vol. 4, no. 8, pp. 647-656, Sept. 2010.

[40] X. Zhu, W. Hua, and Q. Sun, "Cogging torque minimization in flux-switching permanent magnet machines by tooth chamfering", *IEEE Energy Conversion Congress and Exposition*, in press, 2016.

[41] W. Fei, P. C. K. Luk, and J. Shen, "Torque analysis of permanent-magnet flux switching machines with rotor step skewing," *IEEE Trans. Magn.*, vol. 48, no. 10, pp. 2664-2673, Oct. 2012.

[42] H. Jia, M. Cheng, W. Hua, Z. Yang, and Y. Zhang. "Compensation of cogging torque for flux-switching permanent magnet motor based on current harmonics injection," *in Proc. IEEE Int. Electric Motor and Drives Conf.*, pp. 286-291, May, 2009.

[43] H. Jia, M. Cheng, W. Hua, W. Zhao, and W. Li. "Torque ripple suppression in flux switching PM motor by harmonic current

injection based on voltage space-vector modulation," *IEEE Trans. Magn.*, vol. 46, no. 6, pp. 1527-1530, 2010.
[44] Z. Q. Zhu, A.S. Thomas, J. T. Chen, and G. W. Jewell, "Cogging torque in flux-switching permanent magnet machines," *IEEE Trans. Magn.*, vol. 45, no. 10, pp. 4708-4711, 2009.
[45] X. F. Zhu, and W. Hua, "Back-EMF waveform optimization of flux-reversal permanent magnet machines," *AIP Advances*, 2016, Accpeted.
[46] H. Jia, M. Cheng, W. Hua, W. Zhao, and W. Li, "Torque ripple suppression in flux-switching pm motor by harmonic current injection based on voltage space-vector modulation," *IEEE Trans. Magn.*, vol. 46, no. 6, pp. 1527-1530, Jun. 2010.
[47] Weizhe Qian, S. K. Panda, and Jianxin Xu, "Torque ripple minimization in PM synchronous motors using iterative learning control," *IEEE Trans. on Power Electr.*, vol. 19, no. 2, pp. 272-279, Mar. 2004.
[48] J. Rodríguez, R. Kennel, J. R. Espinoza, M. Trincado, C. A. Silva, and C. A. Rojas, "High- performance control strategies for electrical drives: An experi- mental assessment," *IEEE Trans. Ind. Electron.*, vol. 59, no. 2, pp. 812-820, Feb. 2012.
[49] Y. Zhang, and H. Yang, "Two-vector-based model predictive torque control without weighting factors for induction motor drives," *IEEE Trans. on Power Electr.*, vol. 31, no. 2, pp. 1381-1390, Feb. 2016.
[50] W. Hua, W. Huang, and F. Yu, "Improved model-predictive-flux-control strategy for three-phase four-switch inverter-fed flux-reversal permanent magnet machine drives," *IET Electric Power Applications*, 2016, Early access.
[51] M. Cheng, F. Yu, K. T. Chau, and W. Hua, "Dynamic performance evaluation of a nine-phase flux-switching permanent-magnet motor drive with model predictive control," *IEEE Trans. Ind. Electron.*, vol. 63, no. 7, pp. 4539-4549, Jul. 2016.
[52] Y. Zhang, H. Yang, and B. Xia, "Model predictive torque control of induction motor drives with reduced torque ripple," *IET Electric Power Applications*, vol. 9, no. 9, pp. 595-604, Jul. 2015.
[53] W. T. Huang, W. Hua, and Y. Feng, "A model predictive current control of flux-switching permanent magnet machines for torque ripple minimization," *AIP Advances*, vol. 7, pp. 056609, 2017.
[54] W. Huang, and W. Hua, "A finite-control-set-based model-predictive-flux-control strategy with iterative learning control for torque ripple minimization of flux-switching permanent magnet machines," *IEEE Vehicle Power and Propulsion Conference (VPPC), Hangzhou, China*,6 pages, 2016.

Gan Zhang was born in Shandong, China, in 1987. He received the B.Sc. and Ph.D. degree in Electrical Engineering from Southeast University, Nanjing, China, in 2011 and 2016, respectively. He is currently a lecturer with School of Electrical Engineering, Southeast University. His research interests include the design and analysis of novel permanent-magnet brushless electrical machines for application in hybrid vehicles.

Wei Hua received B.Sc. and Ph.D. degrees in Electrical Engineering from Southeast University, Nanjing, China, in 2001 and 2007, respectively. Since 2007, he has been with Southeast University, where he is currently a Professor with the School of Electrical Engineering. He is the author or coauthor of over 140 technical papers, and he is the holder of 30 patents in his areas of interest. His teaching and research interests include the design, analysis, and control of electrical machines.

Ming Cheng, FIEEE and FIET, received the B.Sc. and M.Sc. degrees from the Department of Electrical Engineering, Southeast University, Nanjing, China, in 1982 and 1987, respectively, and the Ph.D. degree from the Department of Electrical and Electronic Engineering, University of Hong Kong, Hong Kong, in 2001.

Since 1987, Prof. Cheng has been with Southeast University, where he is currently a Professor at the School of Electrical Engineering. His teaching and research interests include electrical machines, motor drives for EV, and renewable energy generation. He has authored or co-authored more than 300 technical papers and 4 books, and is the holder of 80 patents in these areas.

Prof. Cheng has served as the Chair and an Organizing Committee Member for many international conferences. He is a Distinguished Lecturer of the IEEE Industry Applications Society for 2015/2016.